

iMacSR: Intermediate Multi-Access Supervision and Regularization in Training Autonomous Driving Models

Wei-Bin Kou¹, Guangxu Zhu³, Yichen Jin¹, Shuai Wang⁴
Ming Tang^{2,*}, and Yik-Chung Wu^{1,*}

Abstract—Deep Learning (DL)-based street scene semantic understanding (S^3U) has become a cornerstone of autonomous driving (AD). DL model performance heavily relies on network depth. Specifically, deeper DL architectures yield better segmentation performance. However, as models grow deeper, traditional one-point supervision at the final layer struggles to optimize intermediate feature representations, leading to subpar training outcomes. To address this, we propose an intermediate Multi-access Supervision and Regularization (iMacSR) strategy. The proposed iMacSR introduces two novel components: (I) mutual information between latent features and ground truth as intermediate supervision loss ensures robust feature alignment at multiple network depths; and (II) negative entropy regularization on hidden features discourages overconfident predictions and mitigates overfitting. These intermediate terms are combined into the original final-layer training loss to form a unified optimization objective, enabling comprehensive optimization across the network hierarchy. The proposed iMacSR provides a robust framework for training deep AD architectures, advancing the performance of perception systems in real-world driving scenarios. In addition, we conduct theoretical convergence analysis for the proposed iMacSR. Extensive experiments on AD benchmarks (*i.e.*, Cityscapes, CamVid, and SynthiaSF datasets) demonstrate that iMacSR outperforms conventional final-layer single-point supervision method up to 9.19% in mean Intersection over Union (mIoU).

I. INTRODUCTION

Autonomous driving (AD) systems rely heavily on precise environmental perception, where street scene semantic understanding (denoted as S^3U) plays a pivotal role in identifying road objects, lanes, drivable areas, etc [1]–[4]. Recent advances in deep learning (DL) have propelled semantic segmentation accuracy to unprecedented levels, with deeper neural networks consistently outperforming shallower counterparts by capturing hierarchical features from complex driving scenes. However, as DL model depth increases, traditional training paradigm of single-point supervision at the network’s output faces inherent limitations, such as gradient vanishing, under-optimized intermediate layers, etc. These limitations often degrade the potential of deep architectures, especially in safety-critical AD applications requiring robustness and generalization.

Current explorations primarily focus on architectural innovations (e.g., residual connections [5], attention mechanisms [6]) to alleviate training difficulties in deep networks. Yet, they overlook the critical role of supervision and regularization strategies in guiding intermediate feature learning. Deeper layers in segmentation models must encode semantically rich, discriminative representations to handle diverse driving conditions (e.g., occlusions, weather variations). Without explicit supervision at intermediate stages, these layers may fail to learn task-relevant features, leading to performance plateaus. Similarly, the absence of regularization on hidden activations risks overconfident predictions, reducing model generalization to unseen scenarios.

To bridge this gap, we propose intermediate Multi-access Supervision and Regularization (iMacSR), a novel training strategy that integrates intermediate multi-point supervision and regularization for training DL-based AD segmentation models. In the proposed iMacSR method, apart from the conventional output-layer supervision, we introduce extra multiple mid-point supervision and regularization from the intermediate layers. For the conventional output-layer supervision, it follows the similar training process with general DL model’s training. For the newly-added intermediate supervision and regularization, we firstly choose multiple intermediate points between the input layer and the output layer of the DL model. We then propose to impose supervision and regularization for all selected intermediate points. Specifically, for each point, we introduce two integral elements: (I) Mutual Information Supervision: We propose to use mutual information between latent features at this point and ground truth as intermediate loss, which is added to the output-supervision loss for optimization. This ensures layers prior to this point encode more meaningful representations than conventional intermediate-supervision-free training method. (II) Negative Entropy Regularization: We propose to calculate negative entropy on latent features at this point, which is added to training loss as a regularizer. This helps to improve generalization by penalizing overconfident hidden feature predictions. In addition, we carry out a theoretical convergence analysis for iMacSR, providing insights into how the intermediate supervision and regularization strategies impact the performance of DL model. The proposed iMacSR is illustrated in Fig. 1. Experiments on Cityscapes [7], CamVid [8], and SynthiaSF [9] datasets demonstrate that iMacSR-trained model achieves 9.19% higher mIoU than conventional baseline.

The main contributions of this work are highlighted as

*Corresponding author: Ming Tang (tangm3@sustech.edu.cn) and Yik-Chung Wu (ycwu@eee.hku.hk).

¹Department of Electrical and Electronic Engineering, The University of Hong Kong, Hong Kong, China.

²Department of Computer Science and Engineering, Southern University of Science and Technology, Shenzhen, China.

³Shenzhen International Center For Industrial And Applied Mathematics, Shenzhen Research Institute of Big Data, Shenzhen, China.

⁴Shenzhen Institutes of Advanced Technology, Chinese Academy of Sciences, Shenzhen, China.

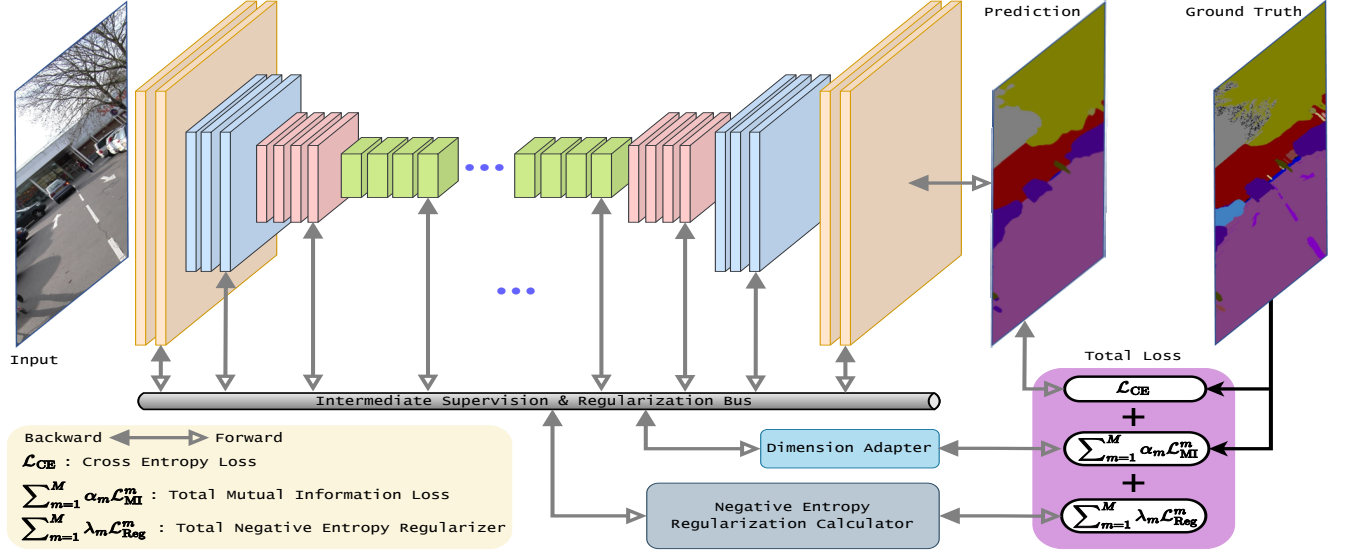


Fig. 1: Overview of the proposed iMacSR training scheme.

follows:

- 1) As DL-based AD models grow deeper, conventional training paradigm relying on single-point supervision at the network's output degrades DL-based AD model performance. To mitigate this issue, we propose iMacSR to improve DL model performance by incorporating intermediate multi-access supervision (mutual information) and regularization (negative entropy).
- 2) We additionally conduct theoretical convergence analysis for iMacSR, which suggests that iMacSR holds $\mathcal{O}(1/\sqrt{T})$ convergence rate that matches standard SGD optimization, proving iMacSR does not harm asymptotic convergence.
- 3) Extensive experiments on multiple datasets demonstrate that iMacSR outperforms conventional training method up to 9.19% in mIoU.

II. RELATED WORK

A. S^3U in AD

Current AD systems are typically divided into two categories: modular-based [10] and learning-based [11]–[13]. Modular-based methods are well-structured but often suffer from error propagation due to inaccuracies in their modeling and problem-solving phases. In contrast, learning-based end-to-end approaches [14] offer a promising alternative by minimizing error propagation. These methods directly transform sensory inputs, such as LiDAR point clouds and camera imagery, into vehicle control actions including throttle, brake, and steering commands. Additionally, learning-based models can be incorporated within modular pipelines. For example, a learning-based model could be used for the S^3U within a semantic segmentation module [15].

S^3U is essential for AD [16]–[20], which assigns a class label to each pixel in an image, facilitating a detailed understanding of the street scene layout, including roads, pedestrians, sidewalks, buildings, and other static and dynamic elements. Modern S^3U methods predominantly rely on

machine learning (ML), particularly DL techniques. Initially, Fully Convolutional Networks (FCNs)-based models brought significant advancements to this task [21]. More recently, Transformer-based approaches [22] have been introduced for semantic segmentation. In general, as the DL-based AD models grow deeper, their inference performance becomes better. However, training these deeper models is a significant challenge for conventional output-layer single-supervision training method owing to decayed gradients, suboptimally tuned latent features, etc. To mitigate this issue, we propose iMacSR to incorporate multiple mid-point supervision and regularization.

B. DL Model Optimization

DL model optimization encompasses a suite of algorithms and techniques designed to optimize a loss function efficiently and effectively across DL model parameters. In general, DL model optimization landscape is complex due to the high dimensionality and non-convex nature of typical loss functions involved in training DL models. Stochastic gradient descent (SGD) lays the groundwork and back-propagation provides a computationally feasible way for training DL models [23]. Based on these two elements, innovations such as Adam [24], RMSprop [25], and AdaGrad [26] later emerged. They offer adaptive learning rates that can resolve some limitations found in SGD, particularly in terms of convergence and stability across various DL model architectures. DL model optimization is also closely linked with techniques intended to improve the generalization and stability of DL models. Regularization strategies such as dropout [27], L1/L2 regularization [28], [29], etc., are critical in preventing overfitting and ensuring robust model performance. Similarly, normalization techniques like batch normalization [30] and layer normalization [31] have been pivotal in stabilizing training. Despite significant advancements, DL model optimization continues to face challenges, particularly in training extremely deep networks. In order

to mitigate this problem, this work presents iMacSR that introduces intermediate multi-point supervision and regularization.

III. METHODOLOGY

We firstly elaborate the proposed iMacSR in Section III-A. We then conduct convergence analysis for the proposed iMacSR in Section III-B. Finally, we discuss the complexity of the proposed iMacSR in Section III-C.

A. The Proposed iMacSR

The key notations in iMacSR formulation are summarized in Table I. Let $\mathcal{D} = \{(x_i, y_i)\}_{i=1}^{|\mathcal{D}|}$ denote the training dataset, where x_i is an input image and y_i is its pixel-wise semantic label. In addition, we set M intermediate supervision and regularization points for the network θ , and such points are denoted as $\{G_1, \dots, G_M\}$. There exist consecutive layers between two adjacent points. For the S³U task, the proposed iMacSR's optimization objective is three-fold:

- Conventional output-layer cross entropy (CE) loss: The standard cross entropy loss is

$$\mathcal{L}_{\text{CE}} = -\frac{1}{|\mathcal{D}|} \sum_{i=1}^{|\mathcal{D}|} \sum_{p \in \Omega} \sum_{k=1}^K y_{i,p,k} \log p_k(x_{i,p}; \theta), \quad (1)$$

where Ω is the pixel set of images, K is the number of semantic classes in dataset \mathcal{D} , and $p_k(x_{i,p}; \theta)$ is the softmax probability at pixel p for class k .

- Intermediate mutual information (MI) loss: For point G_m , the latent feature for the x_i is defined as $z_i^m = \theta^{G_m}(x_i)$. We maximize mutual information between z^m and labels y via

$$\mathcal{L}_{\text{MI}}^m = -\frac{1}{|\mathcal{D}|} \sum_{i=1}^{|\mathcal{D}|} \sum_{p \in \Omega} \sum_{k=1}^K y_{i,p,k} \log q_k^m(z_{i,p}^m; \phi_m), \quad (2)$$

where $q_k^m(\cdot; \phi_m)$ is a dimension adapter with parameters ϕ_m for point G_m , aligning the latent features' dimension with ground truth's dimension for calculating MI.

- Intermediate negative entropy (NE) regularization: For point G_m , to prevent overconfidence of feature representation, we maximize negative entropy of z^m to encourage the model to be less uncertain about its predictions. NE regularizer is formulated as

$$\mathcal{L}_{\text{Reg}}^m = \frac{1}{|\mathcal{D}|} \sum_{i=1}^{|\mathcal{D}|} \sum_{p \in \Omega} \sum_{k=1}^{C_m} p_k^m(z_{i,p}^m; \theta) \log p_k^m(z_{i,p}^m; \theta), \quad (3)$$

where $p_k^m(z_{i,p}^m; \theta)$ is the softmax probability at pixel p for class k , for the intermediate point G_m .

In summary, the total optimization objective is

$$\mathcal{L}_{\text{T}} = \mathcal{L}_{\text{CE}} + \sum_{m=1}^M (\alpha_m \mathcal{L}_{\text{MI}}^m + \lambda_m \mathcal{L}_{\text{Reg}}^m), \quad (4)$$

where α_m, λ_m are coefficients of supervision loss and regularization term, respectively, for point G_m .

TABLE I: Key Notations of iMacSR Formulation

Symbols	Definitions
\mathcal{D}	Training dataset
(x_i, y_i)	Input image and pixel-wise semantic label pair
θ	Segmentation model with parameters θ
M	Total number of intermediate points
G_m	Intermediate supervision and regularization point m
z^m	Latent feature maps at point G_m
C_m	The number of channel of z^m
$p_k(x_i; \theta)$	Softmax probability for class k at the output layer
q_k^m	Dimension adapter for G_m with parameters ϕ_m
\mathcal{L}_{CE}	Cross-entropy loss
$\mathcal{L}_{\text{MI}}^m$	Mutual information loss for point G_m
$\mathcal{L}_{\text{Reg}}^m$	Negative entropy regularization for point G_m
α_m, λ_m	Loss weights for point G_m
η	Learning rate
T	Total training epochs
B	Batch size
K	The number of semantic classes in dataset \mathcal{D}

As usual, the proposed iMacSR optimizes the DL model via gradient descent with the following steps: (I) Forward Pass: For an input image x_i , it computes features $\{z_i^1, \dots, z_i^M\}$ at each point G_m and the final prediction probability $p_k(x_{i,p}; \theta)$. (II) Loss Computation: It calculates the total loss \mathcal{L}_{T} using Eq. (4), which includes \mathcal{L}_{CE} , $\{\mathcal{L}_{\text{MI}}^m\}_{m=1}^M$, and $\{\mathcal{L}_{\text{Reg}}^m\}_{m=1}^M$. (III) Back Propagation: It computes gradients of \mathcal{L}_{T} with respect to DL model parameters θ and auxiliary dimension adapter $\{\phi_m\}$. (IV) Parameter Update: It updates θ and $\{\phi_m\}$ using the Adam optimizer, *i.e.*,

$$\theta \leftarrow \theta - \eta \nabla_{\theta} \mathcal{L}_{\text{T}}, \quad \phi_m \leftarrow \phi_m - \eta \nabla_{\phi_m} \mathcal{L}_{\text{T}}, \quad (5)$$

where η is the learning rate.

In conclusion, iMacSR is outlined in Algorithm 1.

B. Convergence Analysis of iMacSR

To conduct convergence analysis, some assumptions are made. Specifically, for each component $s \in \{\text{CE}, \{\text{MI}\}, \{\text{Reg}\}\}$, \mathcal{L}_s satisfies:

- L-smoothness: There exists $L_s > 0$ such that $\forall \theta, \theta', \|\nabla \mathcal{L}_s(\theta) - \nabla \mathcal{L}_s(\theta')\| \leq L_s \|\theta - \theta'\|$;
- Bounded Gradients: There exists $G_s > 0$ such that $\forall \theta, \mathcal{B}, \mathbb{E}[\|\nabla \mathcal{L}_s(\theta; \mathcal{B})\|^2] \leq (G_s)^2$;
- Bounded Variance: There exists $(\sigma_s)^2 > 0$ such that $\forall \theta, \mathcal{B}, \mathbb{E}[\|\nabla \mathcal{L}_s(\theta; \mathcal{B}) - \nabla \mathcal{L}_s(\theta)\|^2] \leq (\sigma_s)^2$.

Based on these assumptions, we can conclude following Theorem 1 about the convergence of the proposed iMacSR.

Theorem 1: Let $L_{\text{max}} = \max(L_{\text{CE}}, \alpha_m L_{\text{MI}}^m, \lambda_m L_{\text{Reg}}^m)$, $G_{\text{T}}^2 = G_{\text{CE}}^2 + \sum_{m=1}^M (\alpha_m^2 (G_{\text{MI}}^m)^2 + \lambda_m^2 (G_{\text{Reg}}^m)^2)$, and $\sigma_{\text{T}}^2 = \sigma_{\text{CE}}^2 + \sum_{m=1}^M (\alpha_m^2 (\sigma_{\text{MI}}^m)^2 + \lambda_m^2 (\sigma_{\text{Reg}}^m)^2)$. After T iterations of training with $\eta_t = \frac{\eta}{\sqrt{T}}$, we have

$$\frac{1}{T} \sum_{t=1}^T \mathbb{E} \|\nabla \mathcal{L}_{\text{T}}(\theta_t)\|^2 \leq \underbrace{\frac{2\Delta}{\eta\sqrt{T}}}_{\text{Initial gap}} + \underbrace{\frac{L_{\text{max}}\eta}{\sqrt{T}} (G_{\text{T}}^2 + \sigma_{\text{T}}^2)}_{\text{Variance terms}}, \quad (6)$$

where $\Delta = \mathcal{L}_{\text{T}}(\theta_0) - \mathcal{L}_{\text{T}}^*$, θ_0 is the initial model parameters, \mathcal{L}_{T}^* is the theoretical optimal loss.

From Theorem 1, we can conclude following insights:

(I) The $\mathcal{O}(1/\sqrt{T})$ rate matches standard non-convex SGD, proving iMacSR does not harm asymptotic convergence. (II)

Algorithm 1: iMacSR

Input : Training dataset \mathcal{D} , model θ with intermediate points $\{G_1, \dots, G_M\}$, learning rate η , epochs T

Output: Trained model θ^*

- 1 Initialize θ with θ_0 , auxiliary dimension adapter $\{\phi_1, \dots, \phi_M\}$, weights $\{\alpha_1, \lambda_1, \dots, \alpha_M, \lambda_M\}$;
- 2 **for** $epoch = 1$ **to** T **do**
- 3 **for** *each batch* $(x_i, y_i) \in \mathcal{D}$ **do**
- 4 // Forward Pass
- 5 $\{z_i^1, \dots, z_i^M\} \leftarrow \theta(x_i)$;
- 6 $p_k(x_i; \theta) \leftarrow \text{Softmax}(\theta(x_i))$;
- 7 // Loss Computation
- 8 $\mathcal{L}_{CE} \leftarrow -\frac{1}{B} \sum_{i=1}^B \sum_{p,k} y_{i,p,k} \log p_k(x_{i,p}; \theta)$;
- 9 **for** $m = 1$ **to** M **do**
- 10 $\mathcal{L}_{MI}^m \leftarrow -\frac{1}{B} \sum_{i=1}^B \sum_{p,k} y_{i,p,k} \log q_k^m(z_{i,p}^m; \phi_m)$;
- 11 $\mathcal{L}_{Reg}^m \leftarrow \frac{1}{B} \sum_{i=1}^B \sum_{p,k} p_k^m(z_{i,p}^m) \log p_k^m(z_{i,p}^m)$;
- 12 **end**
- 13 $\mathcal{L}_T \leftarrow \mathcal{L}_{CE} + \sum_{m=1}^M (\alpha_m \mathcal{L}_{MI}^m + \lambda_m \mathcal{L}_{Reg}^m)$;
- 14 // Back propagation & Update
- 15 Compute $\nabla_{\theta} \mathcal{L}_T, \nabla_{\phi_m} \mathcal{L}_T$ for all m ;
- 16 **for** $m = 1$ **to** M **do**
- 17 $\phi_m \leftarrow \phi_m - \eta \nabla_{\phi_m} \mathcal{L}_T$;
- 18 **end**
- 19 $\theta \leftarrow \theta - \eta \nabla_{\theta} \mathcal{L}_T$;
- 20 **end**
- 21 **return** θ^*

The gradient bound is positively related to the number of intermediate points (*i.e.*, M), which is controllable via the number selection of intermediate point (e.g., $M = \mathcal{O}(\log D)$ for DL model depth D).

This theorem can be proven by following steps:

- 1) Decompose Total Gradients:

$$\nabla \mathcal{L}_T = \nabla \mathcal{L}_{CE} + \sum_{m=1}^M (\alpha_m \nabla \mathcal{L}_{MI}^m + \lambda_m \nabla \mathcal{L}_{Reg}^m). \quad (7)$$

- 2) Apply L-smoothness per Component:

$$\mathcal{L}_s(\theta_{t+1}) \leq \mathcal{L}_s(\theta_t) + \langle \nabla \mathcal{L}_s(\theta_t), \theta_{t+1} - \theta_t \rangle + \frac{L_s}{2} \|\theta_{t+1} - \theta_t\|^2. \quad (8)$$

- 3) Sum Over All Components:

$$\mathcal{L}_T(\theta_{t+1}) \leq \mathcal{L}_T(\theta_t) - \eta_t \|\nabla \mathcal{L}_T(\theta_t)\|^2 + \frac{\eta_t^2 L_{\max}}{2} (G_T^2 + \sigma_T^2). \quad (9)$$

- 4) Sum the inequality from Step 3) over $t = 1$ to T :

$$\begin{aligned} \sum_{t=1}^T \mathbb{E}[\mathcal{L}_T(\theta_{t+1})] &\leq \sum_{t=1}^T \mathbb{E}[\mathcal{L}_T(\theta_t)] - \eta \sum_{t=1}^T \frac{\mathbb{E}[\|\nabla \mathcal{L}_T(\theta_t)\|^2]}{\sqrt{T}} + \\ &\quad \frac{L_{\max} \eta^2}{2T} \sum_{t=1}^T (G_T^2 + \sigma_T^2). \end{aligned} \quad (10)$$

- 5) Cancel telescoping terms on the LHS/RHS for Step 4):

$$\mathbb{E}[\mathcal{L}_T(\theta_{T+1})] - \mathbb{E}[\mathcal{L}_T(\theta_1)] \leq -\frac{\eta}{\sqrt{T}} \sum_{t=1}^T \mathbb{E}[\|\nabla \mathcal{L}_T(\theta_t)\|^2] + \frac{L_{\max} \eta^2}{2} (G_T^2 + \sigma_T^2). \quad (11)$$

- 6) Rearrange to compute average gradient norm:

$$\begin{aligned} \frac{1}{T} \sum_{t=1}^T \mathbb{E}[\|\nabla \mathcal{L}_T(\theta_t)\|^2] &\leq \frac{\mathbb{E}[\mathcal{L}_T(\theta_1) - \mathcal{L}_T(\theta_{T+1})]}{\eta \sqrt{T}} \\ &\quad + \frac{L_{\max} \eta}{2\sqrt{T}} (G_T^2 + \sigma_T^2). \end{aligned} \quad (12)$$

Bounding $\mathbb{E}[\mathcal{L}_T(\theta_1) - \mathcal{L}_T(\theta_{T+1})] \leq \Delta = \mathcal{L}_T(\theta_0) - \mathcal{L}_T^*$ gives the Eq. (6) (*i.e.*, **Theorem 1**), where θ_0 is the initial model parameters, and \mathcal{L}_T^* is the theoretical optimal loss.

C. Complexity Analysis

To clearly conduct complexity analysis, we denote some notations as follows: D is the depth of the DL-based S^3U model, W and H are the width and the height of the input image, w_m and h_m are the width and the height of the latent feature maps at point G_m .

1) *Time Complexity*: For each batch, the time is composed of three parts: forward time, loss computation time, and backward time. We can formulate each part as follows:

- Forward time: We suppose that the forward time of each layer is approximately same, therefore, the total forward time is $\mathcal{O}(D)$. In addition, we suppose that the feature caching time and dimension adapting time of each point is also same, thus, the total caching time is $\mathcal{O}(M)$. In a nutshell, the total forward time is $\mathcal{O}(D + M)$.
- Loss computation time: In the proposed iMacSR, the total loss includes three components, and we suppose the computation time for each pixel is almost the same. Therefore, the computation time of CE loss is $\mathcal{O}(BWHK)$, the computation time of M intermediate points' MI time is $M \cdot \mathcal{O}(BWHK)$, the computation time of M intermediate points' NE time is $\mathcal{O}(\sum_{m=1}^M Bw_m h_m C_m)$. In summary, the total loss computation time is $\mathcal{O}(BWHK) + M \cdot \mathcal{O}(BWHK) + \mathcal{O}(\sum_{m=1}^M Bw_m h_m C_m) = \mathcal{O}(B((M+1)WHK + \sum_{m=1}^M Bw_m h_m C_m))$.
- Backward time: For backward process, the gradients of CE loss and the gradients of intermediate losses are propagated simultaneously. Therefore, we can treat the backward time of CE gradients as the total backward time. We also suppose the backward time of each layer is the same. Thus, the total backward time is $\mathcal{O}(D)$.

In conclusion, the total time of each batch is $\mathcal{O}(D + M) + \mathcal{O}(B((M+1)WHK + \sum_{m=1}^M Bw_m h_m C_m)) + \mathcal{O}(D)$.

2) *Space Complexity*: Compared to conventional training scheme, the proposed iMacSR has two extra space consumption parts: latent feature cache and auxiliary dimension adapter. The detailed space consumption of both parts are elaborated as follows:

TABLE II: Hardware/Software configurations

Items	Configurations
CPU	AMD Ryzen 9 3900X 12-Core
GPU	NVIDIA GeForce 3090 $\times 2$
RAM	DDR4 32G
DL Framework	PyTorch @ 1.13.0+cu116
GPU Driver	470.161.03
CUDA	11.4
cuDNN	8302

- **Latent feature storage:** To calculate the NE regularization terms, we cache the latent features of each intermediate point. The space for computing NE is $O(\sum_{m=1}^M Bw_m h_m C_m)$. To calculate the MI losses, we cache the outputs of dimension adapter. This space for computing MI is $O(M \cdot BWHK)$. Thus, the total space for latent feature storage is $O(\sum_{m=1}^M Bw_m h_m C_m + M \cdot BWHK)$.
- **Auxiliary dimension adapter:** We suppose each lightweight dimension adapter q_k^m adds $O(P_m)$ parameters. The total space for M intermediate points is $O(\sum_{m=1}^M P_m)$.

In summary, the total extra space for the proposed iMacSR is $O(\sum_{m=1}^M Bw_m h_m C_m + M \cdot BWHK + \sum_{m=1}^M P_m)$.

3) *Discussion of iMacSR Complexity:* Based on above time and space complexity analyses, we can find that iMacSR introduces linear overheads with respect to M for both time and space. For typical configurations (e.g., $M \leq 5$, $K \leq 512$), this overhead is marginal compared to gain in performance. In practice, choosing M proportional to $\log D$ balances overhead and performance.

IV. EXPERIMENTS

In this section, we evaluate the iMacSR training method on the S³U task. We compare the performance enhancement of the proposed iMacSR method against traditional final-layer supervision training approach. This comparison is based on widely recognized and accepted datasets, model architectures, and metrics.

A. Datasets, Evaluation Metrics, and Implementation

1) *Datasets:* The **Cityscapes** dataset [7] consists of 2,975 training images and 500 validation images, each annotated with masks. This dataset encompasses 19 semantic classes, such as vehicles and pedestrians. The **CamVid** dataset [8] comprises a total of 701 samples across 11 semantic classes. For our experiments, we randomly selected 600 samples for training and used the remaining 101 samples as a test dataset. The **SynthiaSF** dataset [9] offers a collection of synthetic, yet photorealistic images that emulate urban driving scenarios. It provides pixel-level annotations for 23 semantic classes, with 1,596 images designated for training and 628 for testing in our studies.

2) *Evaluation Metrics:* We assess the proposed iMacSR on the S³U task using four key metrics: **mIoU**, **mPrecision** (**mPre for short**), **mRecall** (**mRec for short**), and **mF1**. These metrics are formulated as follows:

TABLE III: Training configurations

Items	Configurations
Loss	nn.CrossEntropyLoss
Optimizer	nn.Adam
Adam Betas	(0.9, 0.999)
Weight Decay	1e-4
Batch Size	8
Learning Rate	3e-4
DNN Models	DeepLabv3+ (ResNet18) [32], TopFormer [33], SeaFormer [34]

$$mIoU = \frac{1}{K} \sum_{k=1}^K IoU_k = \frac{1}{K * N} \sum_{k=1}^K \sum_{n=1}^N \frac{TP_{n,k}}{FP_{n,k} + TP_{n,k} + FN_{n,k}},$$

$$mPre = \frac{1}{K} \sum_{k=1}^K Pre_k = \frac{1}{K * N} \sum_{k=1}^K \sum_{n=1}^N \frac{TP_{n,k}}{FP_{n,k} + TP_{n,k}},$$

$$mRec = \frac{1}{K} \sum_{k=1}^K Rec_k = \frac{1}{K * N} \sum_{k=1}^K \sum_{n=1}^N \frac{TP_{n,k}}{TP_{n,k} + FN_{n,k}},$$

$$mF1 = \frac{1}{K} \sum_{k=1}^K F1_k = \frac{1}{K} \sum_{k=1}^K \frac{2 * Pre_k * Rec_k}{Pre_k + Rec_k}, \quad (13)$$

where TP , FP , TN , and FN represent True Positive, False Positive, True Negative, and False Negative, respectively. K denotes the number of semantic classes in the dataset, which is 19 for the Cityscapes dataset, 11 for the CamVid dataset, and 23 for the SynthiaSF dataset. Similarly, N indicates the size of the test dataset, amounting to 500 for the Cityscapes dataset, 101 for the CamVid dataset, and 628 for the SynthiaSF dataset.

3) *Implementation Details:* The primary hardware and software configurations for our experiments are provided in Table II, and the detailed training parameters are outlined in Table III. Our experiments include a comparative analysis of the proposed iMacSR training method against traditional training approach across three models—DeepLabv3+, TopFormer, and SeaFormer—on three datasets, namely Cityscapes, CamVid, and SynthiaSF.

B. Main Results and Empirical Analysis

1) *Quantitative Performance Comparison:* We carry out a bunch of experiments to compare the quantitatively performance of the proposed iMacSR training method against conventional final-layer supervised training method on CNN-based DeepLabv3+ model, and Transformer-based SeaFormer and TopFormer models. The results for all adopted models are presented in Table IV. From Table IV, we can conclude following insights: (I) The proposed iMacSR exceeds the traditional final-layer supervision training method in performance for all adopted models across almost all metrics on Cityscapes, CamVid, and SynthiaSF datasets. This effectively demonstrates the superiority of the proposed iMacSR. Taking the combination of DeepLabv3+ model and Cityscapes dataset as an example, the proposed iMacSR outperforms the traditional training method by margins of $(47.78 - 43.76) / 43.76 \% = 9.19\%$, $(56.28 - 50.40) / 50.40 \% = 11.67\%$, $(59.64 - 51.54) / 51.54 \% = 15.72\%$, and $(55.64 - 50.77) / 50.77 \% = 9.59\%$ in mIoU, mF1, mPrecision, mRecall, respectively. This great enhancement in performance can be further visually confirmed in Fig. 2.

TABLE IV: The quantitative performance comparison of iMacSR against conventional training method for all adopted models

Models	Training Methods	Cityscapes Dataset (%)				CamVid Dataset (%)				SynthiaSF Dataset (%)			
		mIoU	mF1	mPrecision	mRecall	mIoU	mF1	mPrecision	mRecall	mIoU	mF1	mPrecision	mRecall
DeepLabv3+	Conventional	43.76	50.40	51.54	50.77	76.02	82.43	83.07	82.46	33.28	37.27	38.98	36.45
	iMacSR (Ours)	47.78	56.28	59.64	55.64	76.13	82.52	83.09	82.57	34.28	39.13	42.74	37.60
SeaFormer	Conventional	27.40	30.99	30.55	32.14	50.69	56.00	55.40	56.89	24.74	29.70	32.68	29.19
	iMacSR (Ours)	29.82	34.19	33.80	35.45	55.83	62.39	64.19	62.54	24.20	29.23	32.20	29.00
TopFormer	Conventional	32.76	37.64	36.92	39.24	63.10	70.22	71.88	70.25	28.37	33.75	36.97	32.99
	iMacSR (Ours)	34.28	39.96	40.41	40.60	66.38	74.50	77.47	73.60	28.70	34.04	37.22	33.20

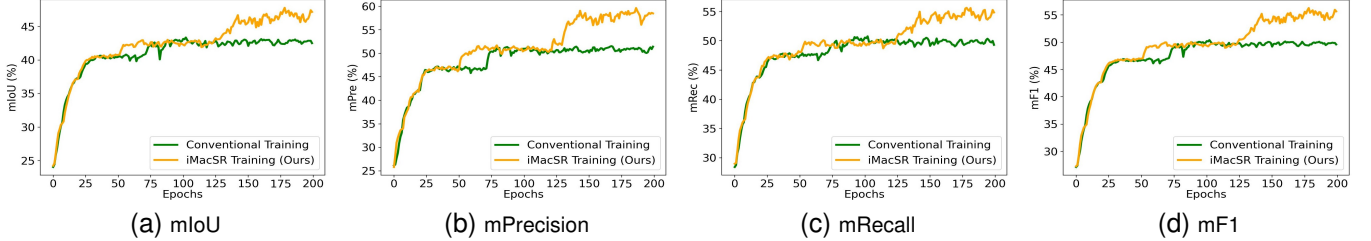
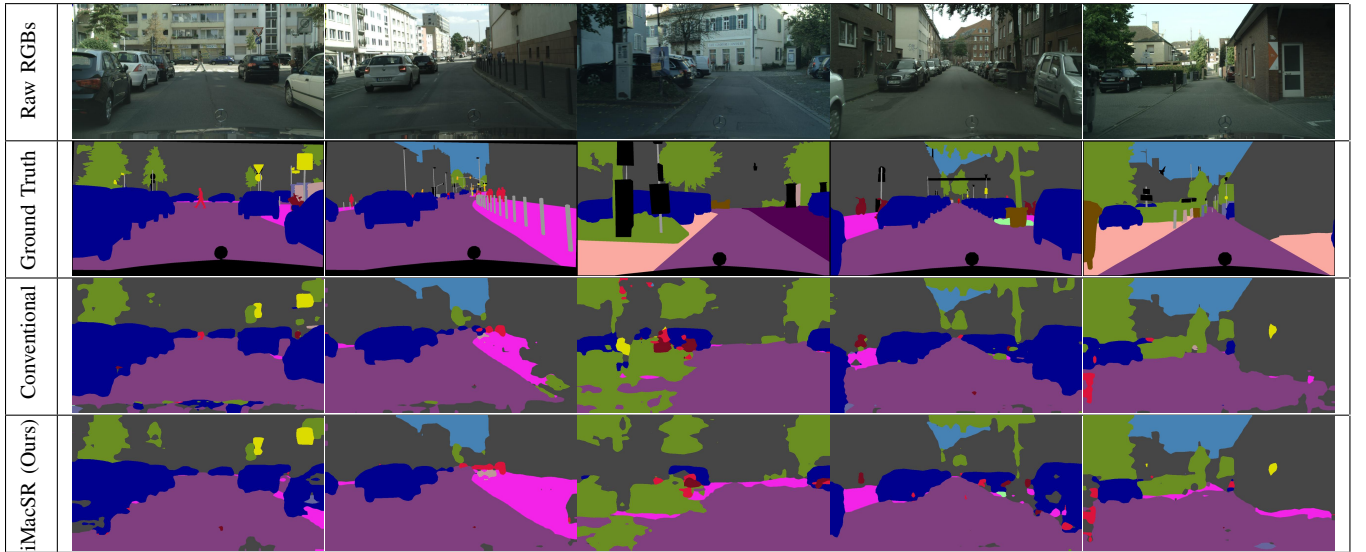


Fig. 2: The visual comparison in performance of iMacSR against the conventional training method for DeepLabv3+ on Cityscapes.

TABLE V: Qualitative performance comparison of the proposed iMacSR against conventional training method



(II) The performance improvement of the proposed iMacSR relative to conventional training method sometimes is related to the complexity of dataset. Specifically, the more complex the dataset, the greater the performance is enhanced. For example, iMacSR improves DeepLabv3+ performance in mIoU by 9.19% on Cityscapes dataset, while by $(76.13 - 76.02) / 76.02 \% = 0.14\%$ and $(34.28 - 33.28) / 33.28 \% = 3.00\%$ on CamVid dataset and SynthiaSF dataset, respectively. (III) The model architecture sometimes also impacts the performance improvement of the proposed iMacSR. For example, on SynthiaSF dataset, the proposed iMacSR can improve the performance of DeepLabv3+ model and TopFormer model, but it fails to improve the SeaFormer model.

2) *Qualitative Performance Comparison:* Table V illustrates the performance of the proposed iMacSR against the conventional training method on five RGB images from diverse AD scenarios. To evaluate the prediction performance of both training methods, we assess how accurately their outputs align with the ground truth and the original images. Our comparison indicates that models trained using iMacSR consistently deliver superior accuracy, capturing both the

broad scene context and intricate details across all images.

C. Ablation Studies

This part reveals three types of ablation studies: (I) how the number of intermediate points affects the performance of iMacSR; (II) how the position of the intermediate points influences the performance of iMacSR; and (III) how the distance between adjacent intermediate points impacts the performance of iMacSR.

1) *The Impact of the Number of Intermediate Points:* To investigate the role of the number of the intermediate points, we compare five cases with different number of intermediate points ranging from 1 to 5, and they are denoted as “Intermediate Point (1)”, “Intermediate Point (2)”, “Intermediate Point (3)”, “Intermediate Point (4)”, “Intermediate Point (5)”, respectively. The comparison result is illustrated in Fig. 3, from which we can observe that cases with both smaller and larger numbers of intermediate points underperform compared to those with a moderate number. This suggests that in practical training, there is no benefit in setting an excessive number of intermediate points between the input

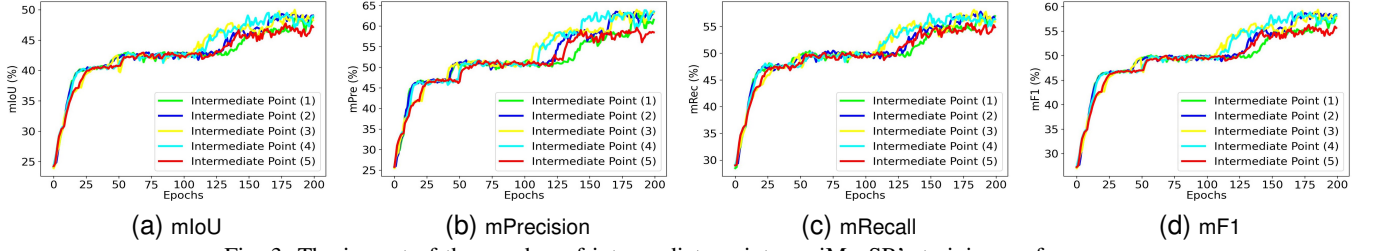
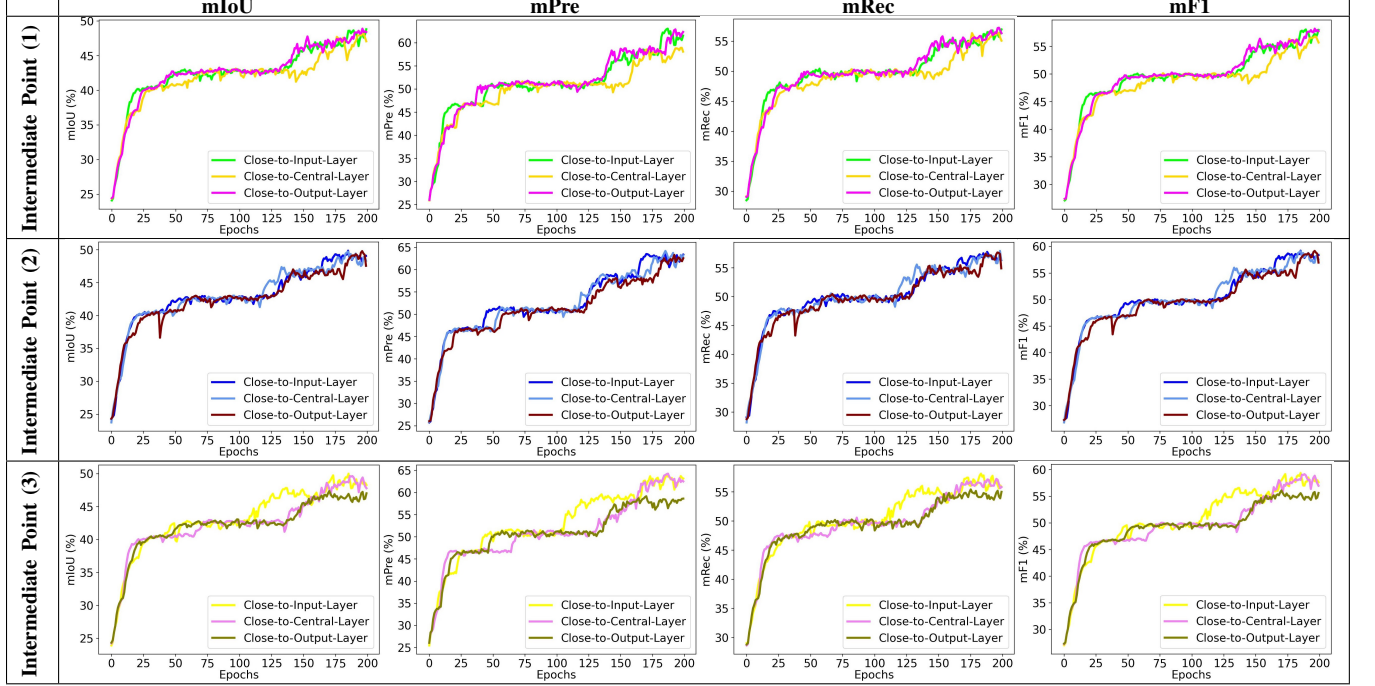


Fig. 3: The impact of the number of intermediate points on iMacSR's training performance.
TABLE VI: The impact of the position of intermediate points on iMacSR's training performance.



and output layers of the DL model.

2) The Impact of the Position of Intermediate Points:

We conducted three series of experiments to investigate the impact of intermediate point placement in a DL model:

- Series I: We place a single intermediate point in three distinct positions: close to the input layer, close to the central layer, and close to the output layer.
- Series II: We position two intermediate points across the same three locations: close to the input layer, close to the central layer, and close to the output layer.
- Series III: We arrange three intermediate points in the aforementioned positions: close to the input layer, close to the central layer, and close to the output layer.

The experimental results are revealed in Table VI. From Table VI, we can figure out following common patterns: (I) For each of these three series, the case of “Close-to-Input-Layer” consistently outperforms cases of “Close-to-Central-Layer” and “Close-to-Output-Layer”. (II) Across all three series, as the number of intermediate points increases, the performance of the case of “Close-to-Output-Layer” progressively deteriorates. (III) Across all three series, increasing the number of intermediate points consistently improves the performance of the case of “Close-to-Central-Layer”.

3) The Impact of the Distance between Intermediate Points:

To figure out how the distance between adjacent intermediate points affects the performance of the proposed iMacSR, we firstly define the base distance as a fixed number of layers between two adjacent layers. Afterwards, we conduct following three experiments by setting the distance between adjacent intermediate points as (I) one base, (II) two bases, and (III) three bases. The experimental results are illustrated in Fig. 4, which indicates that the case with two-base distance achieves the best performance among aforementioned three cases. This inspires us that in training a moderate distance facilitates a better training performance.

V. CONCLUSION

In this study, we address the problem of suboptimal training in DL models for AD due to inadequate supervision for deeper model architectures. We introduce iMacSR strategy to enhance the DL model optimization. iMacSR integrates mutual information for robust intermediate supervision and negative entropy regularization to prevent overconfident predictions. Our experiments demonstrate that iMacSR effectively improves the performance of DL models across various driving scenarios, outperforming traditional final-layer supervision method. Future work will extend iMacSR to

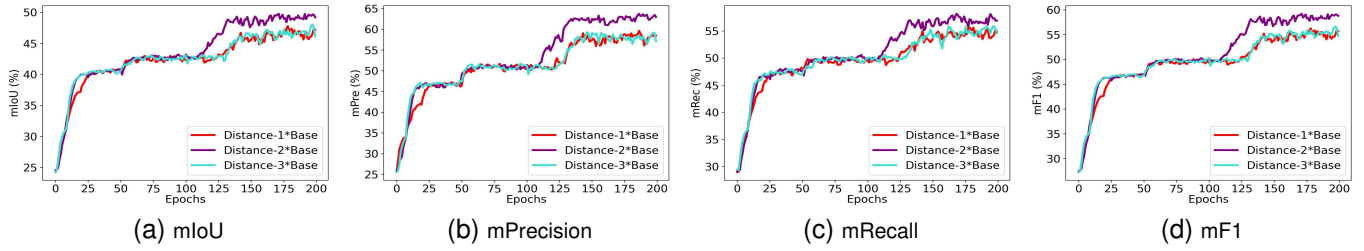


Fig. 4: The impact of the distance between adjacent intermediate points on iMacSR's training performance.

broader AD applications and refine the supervision weights for optimal training outcomes.

REFERENCES

- [1] J. Rückin, F. Magistri, C. Stachniss, and M. Popović, "Semi-supervised active learning for semantic segmentation in unknown environments using informative path planning," *IEEE Robotics and Automation Letters*, vol. 9, no. 3, pp. 2662–2669, 2024.
- [2] W.-B. Kou, G. Zhu, R. Ye, S. Wang, M. Tang, and Y.-C. Wu, "Label anything: An interpretable, high-fidelity and prompt-free annotator," *arXiv preprint arXiv:2502.02972*, 2025.
- [3] Z. Feng, Y. Guo, and Y. Sun, "Cekd: Cross-modal edge-privileged knowledge distillation for semantic scene understanding using only thermal images," *IEEE Robotics and Automation Letters*, vol. 8, no. 4, pp. 2205–2212, 2023.
- [4] W.-B. Kou, Q. Lin, M. Tang, S. Wang, R. Ye, G. Zhu, and Y.-C. Wu, "Enhancing large vision model in street scene semantic understanding through leveraging posterior optimization trajectory," *arXiv preprint arXiv:2501.01710*, 2025.
- [5] K. He, X. Zhang, S. Ren, and J. Sun, "Deep residual learning for image recognition," in *Proceedings of the IEEE conference on computer vision and pattern recognition*, 2016, pp. 770–778.
- [6] A. Vaswani, N. Shazeer, N. Parmar, J. Uszkoreit, L. Jones, A. N. Gomez, Ł. Kaiser, and I. Polosukhin, "Attention is all you need," *Advances in neural information processing systems*, vol. 30, 2017.
- [7] M. Cordts, M. Omran, S. Ramos, T. Rehfeld, M. Enzweiler, R. Benenson, U. Franke, S. Roth, and B. Schiele, "The cityscapes dataset for semantic urban scene understanding," in *Proc. of the IEEE Conference on Computer Vision and Pattern Recognition (CVPR)*, 2016.
- [8] G. J. Brostow, J. Shotton, J. Fauqueur, and R. Cipolla, "Segmentation and recognition using structure from motion point clouds," in *Proc. European Conference on Computer Vision of the (ECCV)*, 2008.
- [9] G. Ros, L. Sellart, J. Materzynska, D. Vazquez, and A. M. Lopez, "The synthia dataset: A large collection of synthetic images for semantic segmentation of urban scenes," in *Proceedings of the IEEE conference on computer vision and pattern recognition*, 2016, pp. 3234–3243.
- [10] Y. Jiang, H. Yedidsion, S. Zhang, G. Sharon, and P. Stone, "Multi-robot planning with conflicts and synergies," *Autonomous Robots*, vol. 43, no. 8, pp. 2011–2032, 2019.
- [11] J. Wu, J. Ruenz, H. Berkemeyer, L. Dixon, and M. Althoff, "Goal-oriented pedestrian motion prediction," *IEEE Transactions on Intelligent Transportation Systems*, vol. 25, no. 6, pp. 5282–5298, 2024.
- [12] M. Herb, N. Navab, and F. Tombari, "Neural semantic map-learning for autonomous vehicles," in *2024 IEEE/RSJ International Conference on Intelligent Robots and Systems (IROS)*, 2024, pp. 1062–1069.
- [13] W.-B. Kou, G. Zhu, R. Ye, S. Wang, Q. Lin, M. Tang, and Y.-C. Wu, "An adverse weather-immune scheme with unfolded regularization and foundation model knowledge distillation for street scene understanding," *arXiv preprint arXiv:2409.14737*, 2024.
- [14] W.-B. Kou, S. Wang, G. Zhu, B. Luo, Y. Chen, D. W. K. Ng, and Y.-C. Wu, "Communication resources constrained hierarchical federated learning for end-to-end autonomous driving," 2023.
- [15] A. Almin, L. Lemarié, A. Duong, and B. R. Kiran, "Navya3dseg - navya 3d semantic segmentation dataset design split generation for autonomous vehicles," *IEEE Robotics and Automation Letters*, vol. 8, no. 9, pp. 5584–5591, 2023.
- [16] Z. Zhengl, Y. Chen, B.-S. Hua, and S.-K. Yeung, "Compuda: Compositional unsupervised domain adaptation for semantic segmentation under adverse conditions," in *2023 IEEE/RSJ International Conference on Intelligent Robots and Systems (IROS)*, 2023, pp. 7675–7681.
- [17] W.-B. Kou, Q. Lin, M. Tang, S. Wang, G. Zhu, and Y.-C. Wu, "Fedrc: A rapid-converged hierarchical federated learning framework in street scene semantic understanding," in *2024 IEEE/RSJ International Conference on Intelligent Robots and Systems (IROS)*. IEEE, 2024, pp. 2578–2585.
- [18] W.-B. Kou, Q. Lin, M. Tang, R. Ye, S. Wang, G. Zhu, and Y.-C. Wu, "Fast-convergent and communication-alleviated heterogeneous hierarchical federated learning in autonomous driving," *IEEE Transactions on Intelligent Transportation Systems*, 2025.
- [19] R. Römer, A. Lederer, S. Tesfazgi, and S. Hirche, "Vision-based uncertainty-aware motion planning based on probabilistic semantic segmentation," *IEEE Robotics and Automation Letters*, vol. 8, no. 11, pp. 7825–7832, 2023.
- [20] W.-B. Kou, Q. Lin, M. Tang, S. Xu, R. Ye, Y. Leng, S. Wang, Z. Chen, G. Zhu, and Y.-C. Wu, "pfedlvm: A large vision model (lvm)-driven and latent feature-based personalized federated learning framework in autonomous driving," *arXiv preprint arXiv:2405.04146*, 2024.
- [21] T. Zhou, W. Wang, E. Konukoglu, and L. Van Gool, "Rethinking semantic segmentation: A prototype view," in *Proceedings of the IEEE/CVF Conference on Computer Vision and Pattern Recognition*, 2022, pp. 2582–2593.
- [22] A. Z. Zhu, J. Mei, S. Qiao, H. Yan, Y. Zhu, L.-C. Chen, and H. Kretzschmar, "Superpixel transformers for efficient semantic segmentation," in *2023 IEEE/RSJ International Conference on Intelligent Robots and Systems (IROS)*, 2023, pp. 7651–7658.
- [23] S.-i. Amari, "Backpropagation and stochastic gradient descent method," *Neurocomputing*, vol. 5, no. 4-5, pp. 185–196, 1993.
- [24] D. P. Kingma and J. Ba, "Adam: A method for stochastic optimization," *arXiv preprint arXiv:1412.6980*, 2014.
- [25] G. Hinton, N. Srivastava, and K. Swersky, "Neural networks for machine learning lecture 6a overview of mini-batch gradient descent," *Cited on*, vol. 14, no. 8, p. 2, 2012.
- [26] J. Duchi, E. Hazan, and Y. Singer, "Adaptive subgradient methods for online learning and stochastic optimization," *Journal of machine learning research*, vol. 12, no. 7, 2011.
- [27] G. E. Hinton, N. Srivastava, A. Krizhevsky, I. Sutskever, and R. R. Salakhutdinov, "Improving neural networks by preventing co-adaptation of feature detectors," *arXiv preprint arXiv:1207.0580*, 2012.
- [28] R. Tibshirani, "Regression shrinkage and selection via the lasso," *Journal of the Royal Statistical Society Series B: Statistical Methodology*, vol. 58, no. 1, pp. 267–288, 1996.
- [29] A. E. Hoerl and R. W. Kennard, "Ridge regression: Biased estimation for nonorthogonal problems," *Technometrics*, vol. 12, no. 1, pp. 55–67, 1970.
- [30] S. Ioffe and C. Szegedy, "Batch normalization: Accelerating deep network training by reducing internal covariate shift," in *International conference on machine learning*. pmlr, 2015, pp. 448–456.
- [31] J. L. Ba, J. R. Kiros, and G. E. Hinton, "Layer normalization," *arXiv preprint arXiv:1607.06450*, 2016.
- [32] L.-C. Chen, Y. Zhu, G. Papandreou, F. Schroff, and H. Adam, "Encoder-decoder with atrous separable convolution for semantic image segmentation," 2018.
- [33] W. Zhang, Z. Huang, G. Luo, T. Chen, X. Wang, W. Liu, G. Yu, and C. Shen, "Topformer: Token pyramid transformer for mobile semantic segmentation," in *Proceedings of the IEEE/CVF Conference on Computer Vision and Pattern Recognition*, 2022, pp. 12 083–12 093.
- [34] Q. Wan, Z. Huang, J. Lu, Y. Gang, and L. Zhang, "Seaformer: Squeeze-enhanced axial transformer for mobile semantic segmentation," in *The eleventh international conference on learning representations*, 2023.